Available online at www.sciencedirect.com

ScienceDirect

journal homepage: http://www.elsevier.com/locate/acme

Original Research Article

Moment capacity and fire protection of the welded plate joint for precast members

Pattamad Panedpojaman *, *Pattharasit Jina*, *Suchart Limkatanyu*

Department of Civil Engineering, Faculty of Engineering, Prince of Songkla University, Songkhla 90110, Thailand

ARTICLE INFO

Article history:
Received 10 December 2015
Accepted 29 April 2016
Available online 1 June 2016

Keywords:
Welded plate joint
Moment capacity
Fire resistance
Load test
Fire test

ABSTRACT

Specimens of reinforced concrete (RC) cantilever beams connected by a welded plate joint to an RC main beam were investigated. Load tests and fire tests were conducted to examine structural behavior and fire resistance of the joint. Under flexural load, the main failure modes of the joint were splitting of the welded plate and rebar yielding. The joint moment capacity depended on ability of the joint to resist tensile forces in the beam rebars. The ultimate loads were about 50% and 70% of corresponding cast-in-place specimens, for the joints with 4-mm and 6-mm thick plates, respectively. To simply estimate the moment capacity, the plate in its width direction was modeled as a beam with fixed ends, and the forces in tensile rebars acted as point loads. The proposed computation of the moment capacity was validated with the tests and with FE simulations, for both moment magnitudes and failure types. By using fire tests, fire protections of the joint such as thin or thick mortar plaster, or a flexible sealant, were investigated. The thick plaster and the sealant provided fire resistances exceeding 2 h. However, the flexible sealant coped better of these two with the separating and swelling behaviors.

1. Introduction

Instead of traditional cast-in-place methods, which are laborious, precast reinforced concrete systems are now widely used in construction to avoid labor costs. Precast concrete members offer various advantages over cast-in-place members [1–3], such as easier implemented overall quality control, ready supply of good quality aggregates, and better quality control of the concrete under factory conditions than at construction site. On the other hand, the joints or connections or precast members are usually problematic. The connection joints can reasonably be considered the weakest most critical points of a precast concrete structure, with concerns about their capacity and stability. The highest priority in this respect is on joints between primary structural members, such as joints of beams and columns or of beams and beams.

Various types of joints are found between precast concrete members used in buildings, and welded joins are widely applied. However, in a welded joint the quality of welding must be under strict control. Welded joints have been developed since 1990 [4,5], and as the simplest cases, the connections of welded plates and billet connectors were investigated early for their structural behavior under monotonic loads [4–6]. These

* *Corresponding author*. Tel.: +66 865971834.
E-mail address: ppattamad@eng.psu.ac.th (P. Panedpojaman).
http://dx.doi.org/10.1016/j.acme.2016.04.017

connections proved satisfactory for semi-rigid designs, as reported in [7].

In typical current practice in Mexico, welded reinforcement is used to connect precast concrete members into moment-resisting frames [8]. Tests under cyclic lateral loading of welded reinforcement type beam-column connections have been conducted [9], and limited inelastic behavior was observed for positive moment. Fracture of the welded reinforcement was observed at a low positive moment after unloading from peak negative moment. In finite element analysis of the connection under cyclic lateral load [8], the beam-column connections with welded longitudinal reinforcement showed local embrittlement of the steel, resulting in brittle failure of the connection.

Ways to connect a precast middle beam and cantilever beams have been developed. These cantilever beams extend out from the columns of a structure, and the precast middle beam is placed on the cantilever beams. Shear and moment capacities of welded lap splicing joints for this type of connection were investigated in [1]. Within the connection region, the top rebars of a beam are continued by lap splicing and its bottom rebars are continued by welding steel plates, for the middle and the cantilever beams. After placing the middle precast beam on the cantilever beams so that the rebars connect, plate welding and concrete casting finish the connection. Load testing of such connection [1] showed improved shear and bending performance.

A type of connection for a precast middle beam and cantilever beams with welded plates has been developed as a dry joint [10,11]. The connections consist of two steel plates at the beam tips, one being at the top and the other at the bottom. These are welded to the steel plates anchored in the precast middle beam. Side surfaces of the members are also welded with steel plates to further connect the members. Based on an experimental investigation [11], these connections performed well under reversed cyclic loading. Strength, stiffness and energy dissipation of such structure were comparable to those of a monolithic member. Very large deformations took place in the members without side plates, and the load carrying capacity was reduced significantly. The side plates were an important part of the connection for resistance to reversed cyclic loads.

As described above, various types of welded joints were found in the literature that describes potential applications of welded systems in connecting precast members. In constructing comparatively light weight buildings, such as houses, warehouses etc., simple precast concrete connections of welded steel plates, as shown in Fig. 1, with or without billet connectors, have been applied for column or beam members. On using welded plate joints, the steel plates are directly welded to reinforcing steel of the precast members, or the steel plates are welded with L shaped dowel bars and embedded in the precast members. The welded plate joint is also considered a dry joint without cast-in-situ concrete. This type of joint is the focus of the current study.

The literature on structural behavior of and design methods for welded plate joints is rather limited. Moment capacities of the joints are of particular concern, due to complicated failure mechanisms. Boonklom [12] investigated the maximum moment capacity and the cyclic behavior of

Fig. 1 – Electric welding of a welded plate joint.

beam-column connections. From experimental results it was concluded that the moment capacities for precast members with welded plate joints and with cast-in-place joints were 0.79 and 0.52 fold, respectively, those of whole cast-in-place members. Thawonpaisanchewa [13] examined the structural behavior of welded plate joints used in beam-column connections, in terms of their failure patterns and moment–rotational angle relationships. Failure of a specimen was initiated by the separation of the welded plate from the precast member. Concrete cracks at the connection gradually propagated with increasing load. Diagonal cracks at the joint were found in the column. Finite element models were used to investigate the force transfer mechanisms at the connections. The results suggested that ductility or efficiency in resisting moment of the beam-column connection could be improved by use of a thicker steel plate in the welded plate joint. However, moment capacity designs for the joint were not provided.

In the literature on welded plate joints, only the influence of plate thickness on the structural behavior has been investigated. The influence of other parameters on structural behavior of the joint is poorly known. Furthermore, fire resistance of the joint has not been examined, while reinforced concrete members can provide fire resistance without fire protection materials. However, the welded plate joints are potentially weak points in the system, since mechanical properties of steel are significantly more degraded by heat than those of concrete. Without fire protection a steel joint might fail quickly in a severe fire. Fire protection of the joints receives only little attention in current construction practice.

To promote safe practices in joints of precast concrete members, this study aimed to investigate their structural behavior and to develop design methods for the moment capacity, through both experimental and numerical investigations. Furthermore, the failure behavior and the fire resistance of such joints were also investigated in this study.

2. Load test experiments

To investigate the failure behavior of welded plate joints, load tests were conducted with seven beam–beam connections. A brief summary of the experimental investigation and the test variables is given in the following.

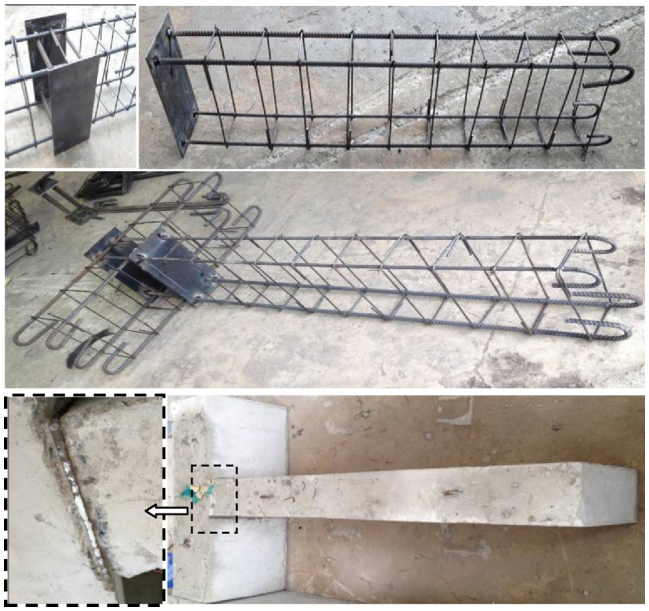

Fig. 2 – A set of the steel reinforcements, and reinforced concrete specimens with welded plate joint.

The test specimens were a set of main reinforced concrete (RC) beams connected to cantilever RC beams by welded plate joints, as shown in Fig. 2. The setup of the load test is depicted in Fig. 3. The dimensions of the main beam were fixed at 300 mm × 400 mm in cross-section, and 1200 mm in overall length. Both ends of the main beams were fixed to supports with steel frames. Each main beam was reinforced with four 16 mm diameter deformed bars (DB). The cantilever beams all had 1600 mm overall length with 6 mm-diameter round bars (RB) as stirrups at 150 mm spacing throughout the beam's length. Steel plates for the welded joints had the dimensions of the cantilever beam cross-section. Symbol identifier, cross-section, reinforcement details and plate thicknesses for each load test case are tabulated in Table 1. Furthermore, to monitor the strain in rebars and plates during load testing, strain gauges with 120 Ω nominal resistance were used, with details of a typical load test shown in Fig. 4.

These beams were cast using the same concrete mixture, with an average 26 MPa compressive strength (standard deviation 1.02 MPa) based on strength tests of five standard cylinders at 28 days after casting. All of the beams were cast and cured at room temperature. After casting the beams were covered with plastic wrap to reduce concrete drying, and were moist-cured for at least 28 days before testing. The load and fire tests of the beams were carried out at the ages of 30–60 days.

The steel rebars with 12 and 16 mm diameters were deformed bars, whereas the smaller diameter ones were round bars. The deformed bars were SD 40 grade with tested tensile yield strengths of 450 MPa and 475 MPa for the 12 and 16 mm diameters, respectively. The round bars were SR 24 grade with tested yield strength of 320 MPa. The steel plates were HR1 grade with tested yield strength of 380 MPa. The modulus of elasticity was approximately 195,000 MPa for the steel rebar and the steel

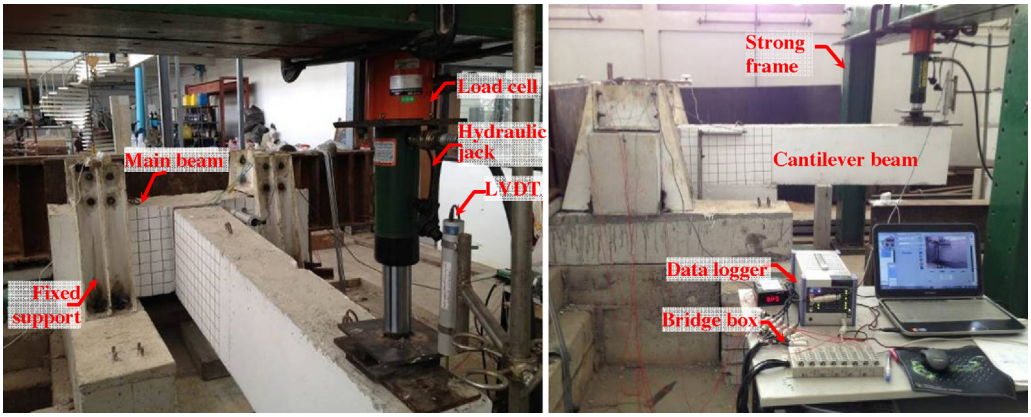

Fig. 3 – Experimental setup for the load test.

Table 1 – Experimental cases in the load tests.

Specimen identifier	Cantilever member ($h \times b$) (mm)	Diameter of reinforcement (mm)		Steel plate thickness (mm)
		Compression	Tension	
A12*	150 × 300	12	12	–
A9-4	150 × 300	12	9	4
A12-4	150 × 300	12	12	4
A12-6	150 × 300	12	12	6
B16*	200 × 400	12	16	–
B16-4	200 × 400	12	16	4
B16-6	200 × 400	12	16	6

Note: *Cast-in-place specimen.

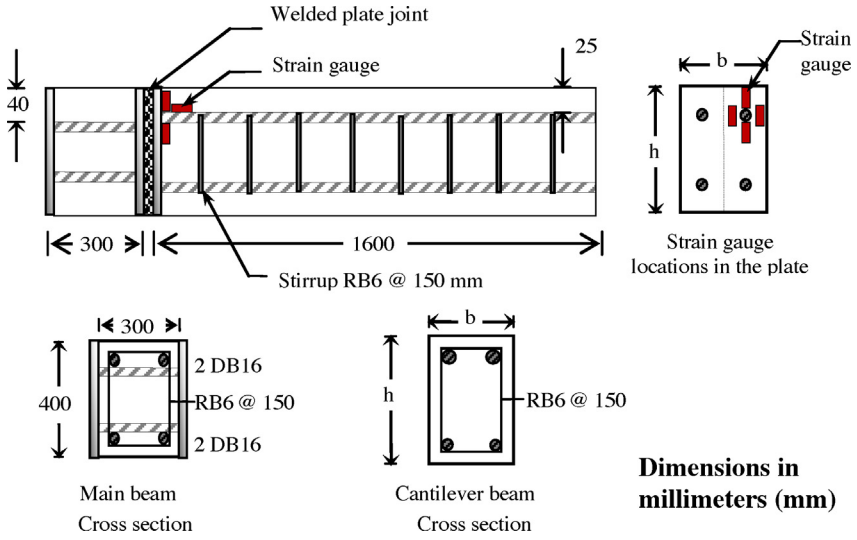

Fig. 4 – Design and instrumentation of a typical test beam.

plates alike. By using E60 electrodes with yield strength of 420 MPa, a 4-mm and 6-mm fillet weld was used for the 4-mm thick plates and the 6-mm thick plates, respectively. The plates were welded along their 4 edges. To avoid damage of the strain gauges during the welding, the plates of the joint were welded before the gauge installations and concrete casting.

Each test beam was supported as illustrated in Fig. 3. The end of the cantilever beam was subjected to a point load applied by a hydraulic jack. The applied load was increased approximately at 0.10–0.20 ton/min rate. To monitor the displacement at the beam end, linear variable differential transducers (LVDT) with an accuracy of 0.1 mm (0.004 in) were installed. The load, the vertical displacement of the beam end, and the strains in the reinforcement and the plate were recorded every two seconds until failure. Deformations and failure behaviors were assessed for the test cases.

3. Experimental results

Failure patterns of the cast-in-place specimen and the specimens with joints are shown in Figs. 5 and 6, respectively. These failure patterns can be explained through structural behavior. The load bearing at the beam end causes a moment along the cantilever beam length, which is maximal at the connection. This moment induces tensile and compressive forces in the rebars and the concrete section in the beam. Due to tensile forces, flexural cracks in the upper concrete section near the connection were observed first. Furthermore, the tensile force induced in the upper rebars was transferred to surrounding concrete through their bonding and caused its cracking. However, the bond cracks first emerged only at the interfaces of rebar and concrete cover, and were not observed at the beam surfaces.

The cast-in-place specimens had higher load resistances than the specimens with joints. With higher tensile forces induced in the upper rebars, the internal bond cracks were larger. Once the flexural cracks linked to the bond cracks, the cracks rapidly propagated, and separation of the cantilever beam from the main beam became clear. For specimen A12 with small rebars, thickness of the concrete cover at the connection was sufficient to resist the forces transferred from the rebars. Therefore, the crack line was confined to the connection, as depicted in Fig. 5(a). Higher tension forces than

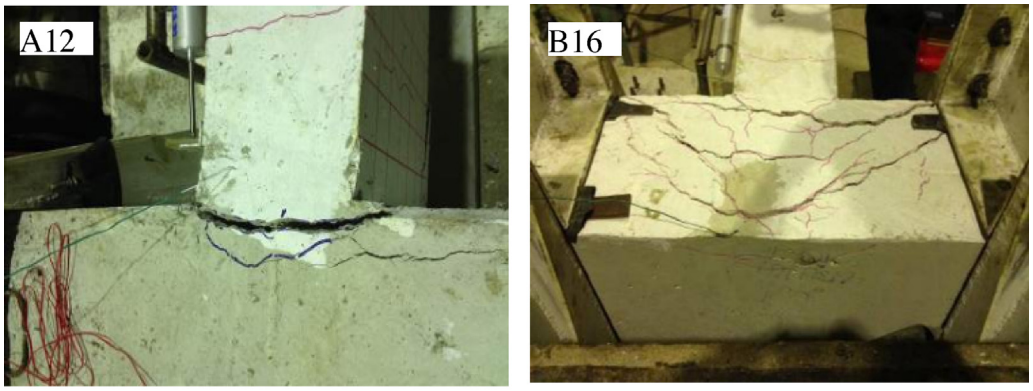

Fig. 5 – Failure patterns in cast-in-place specimens: (a) specimen A12, and (b) specimen B16.

Fig. 6 – Failure patterns of the welded plate joint: (a) welded plate failure, (b) steel reinforcement yielding, and (c) welding failure at the reinforcement.

those in specimen A12 were generated in cases with larger rebars, specimen B16. In such cases, thickness of the concrete cover could not resist the forces from the rebars, and the bond cracks spread out into the main beam. The crack line was first observed at the connection, and later extended to the main beam as a cone failure, shown in Fig. 5(b).

In cases with a welded plate joint, the tensile forces in the steel rebars of the cantilever beam indirectly transferred to the main beam through the welded plate joint. The load bearing capacity depended on the ability to transfer loads at the joint. In addition to shear forces, upper plates of the joint were under opposite pulling forces due to the tensile force transfer, as shown in Fig. 6(a) and (b). As the load increased, first a very small separation between the cantilever beam, the welded plate and the main beam emerged. Later, the welded plate swelled and small cracks were observed in some cases. The deflection developed quickly after the plate swelling, and at the ultimate load welding around the plate edge was split at the upper part, corresponding to the tensile forces. Such welded plate failure is seen in Fig. 6(a). This failure type was dominant in cases with the joint. However, the joint failure in case A9-4 was due to yielding in the tensile rebars, observed with strain gauges and from the concrete cracking near the joint, as shown in Fig. 6(b). Welding failure between the tensile rebars and the plate was found in case A12-6, as shown in Fig. 6 (c), where the plate swelling was very small, and load transfer at the joint was not complete: the failure could be due to poor quality of the welding. The types of joint failure are summarized in Table 2.

The load responses recorded by instrumentation are shown in Fig. 7. It is seen in Fig. 7(a) that the ultimate load of specimens with a welded joint and 4 mm plate was about 50% of the cast-in-place case, while the 6 mm plate gave similarly 70% ultimate strength. The slope of a load–deflection curve represents stiffness of the joint, and the initial stiffnesses were closely similar to the cast-in-place cases for the thicker plate, but was degraded for the thinner plate. Separation of RC members at the joint may have caused the degradation in stiffness. The load–deflection curves of cases A9-4, A12-4 and A12-6 indicate that the stiffness mainly increased with the plate thickness while the diameter of reinforcement had little effect.

The load–strain curves of the tensile rebars are shown in Fig. 7(b). It is clear that the rebars of all specimens, except for the case A9-4, did not reach their yield stress. Therefore, flexural failure in the beam section did not occur, instead the failure was mainly due to concrete cracking (for the cast-in-place specimens) or joint failure (for other cases). However, the case A9-4 had small rebar, so tensile forces from the rebars acting on the welded plate joint were below the joint strength, so the joint resisted the tensile forces until yield in the rebars.

The load–average strain curves are shown in Fig. 7(c) for the steel plate around the tension rebars. Strain measured at such locations normally indicates large swell due to tension forces. However, the strains observed were very low compared to those in reinforcing steel or to yield strain. This indicates that the failure was not directly caused by stresses in the plate, at least at the location observed. The failure pattern may involve swelling of the plate in the elastic region.

4. Finite element analysis simulations

The finite element (FE) method has been widely used to study the inelastic failure of RC beams. To simulate structural behavior of the specimens by FE, the commercial software ANSYS was used. Due to symmetry of the test setup, the FE

Table 2 – Summary of failure types.

Specimen	Type of failure
A12	Concrete crack
B16	Concrete crack
A9-4	Rebar yielding
A12-4	Welded plate failure
A12-6	Welding failure at the rebar
B16-4	Welded plate failure
B16-6	Welded plate failure

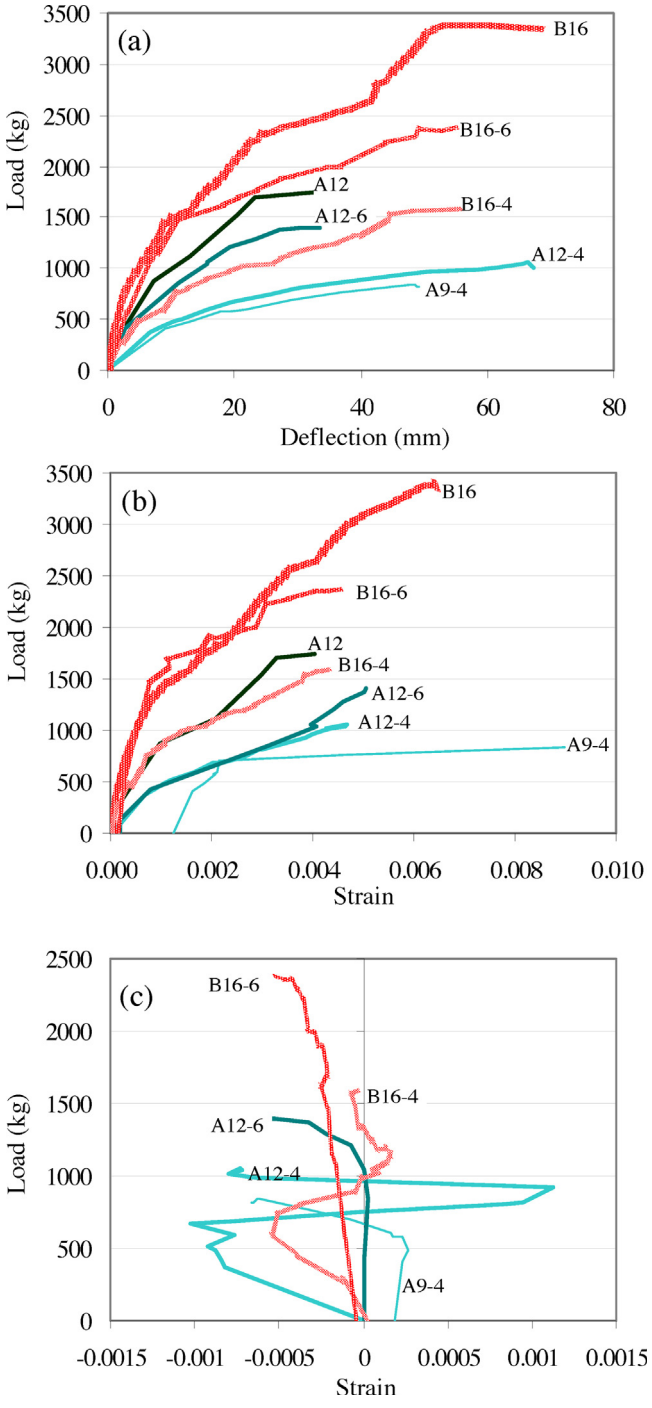

Fig. 7 – Load responses across all cases: (a) load vs. deflection, (b) load vs. strain of tension reinforcement, and (c) load vs. strain of steel plate.

model involved only one half of each specimen, as shown in Fig. 8. The numerical simulation of the specimens was subdivided into two parts to simulate the imposed loading sequences in the test. First the beam model was subjected only to its own weight, reaching equilibrium stress and strain, and in the second part the external loading was incrementally applied until structural failure occurred.

The FE model used for this structural analysis [14] included the solid elements Solid65 to model concrete; the Solid45 elements to model rebars in the cantilever beam and the welded plate joint; for bar elements Link8 was used to model the stirrups and rebars in the main beam; and for contact elements Conta173 was used to model contacting surfaces of the concrete and the steel plate. The solid element Solid65 is capable of modeling concrete cracking in tension, based on the smeared crack theory. The solid element Solid45 is capable of modeling plasticity, swelling, stress stiffening, large deflections, and large strains. The deformation of the elements (Solid65 and Solid45) is characterized by eight nodes, each having three degrees of freedom, namely for displacements in the x, y, and z directions. The 2-node bar element Link8 is a uniaxial tension–compression element with three degrees of freedom at each node: displacements in the x, y, and z directions. The Link8 element is capable of modeling bars with plasticity and large deflections. The contact element Conta173 is applicable to coupled field contact analyses, and shares the geometric characteristics of the solid element face with which it is connected. The contact analysis is effective when the element surface penetrates another element on a specified surface. For the investigated specimens, penetration occurred around the bottom part of the joint, in which the compression force is transferred between the cantilever beam, the joint and the main beam.

The bond–slip relationship at the concrete–rebar interface was modeled as perfect bond through connections between the solid concrete elements and the steel bar elements. The concrete element and the rebar element were set to share the same nodes at the connection. The FE models had simple supports at the main beam ends, and the vertical displacements u_y were restrained at the bottom surface of the support as shown in Fig. 8. The lateral displacements u_z are restrained at the other surfaces of the support. Symmetry boundary condition was set at the symmetry plane. The load was applied by a group of point loads at the cantilever beam end.

The tensile stress–strain relationship for steel was adopted based on tested properties (i.e., yield strength and elastic modulus). To conservatively evaluate the failure load in the nonlinear analysis, a linear elastic modulus with perfectly plastic stage after yield was specified; strain hardening of modulus after yield was not considered. The stress–strain relationship for concrete in compression was assumed to follow the normalized stress–strain relationship of BS EN 1992-1-2 [15] until the peak stress is reached, and to be perfectly plastic thereafter. This assumption enhanced the stability of the finite element simulations. The tensile strength of concrete was specified as 10% of the compressive strength. The shear transfer coefficients for the opening and the closing cracks of concrete were set to 0.30 and 0.50, respectively [16]. The Poisson's ratio was fixed at 0.3 and 0.2 for the steel and the concrete, respectively.

For the non-linear analysis, the Newton–Raphson iterative method was used to identify the failure load. The load step was controlled by time step analysis, which was gradually applied at 50 step increments. However, in order to achieve convergence, size of the load increments was automatically varied when the failure load was approached. The convergence criteria based on force equilibriums and displacement

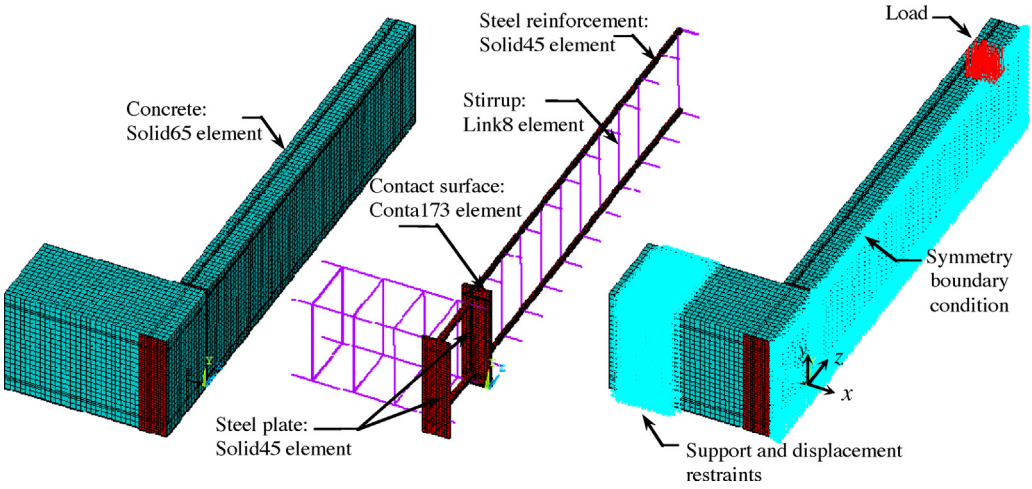

Fig. 8 – Finite element models.

compatibilities were used to define the termination of numerical simulation.

The load–deflection curves, the load–rebar strain curves and the load–steel plate strain curves of the specimens obtained from the physical experiments are compared with the results from the FE numerical simulations in Figs. 9–11. The comparison reveals that the numerical simulation results are consistent with the experimental ones. The simulated plate strain in the figure appears very low compared to the reinforcing steel's strain.

It is observed that the initial slope of the load–deflection curves and the load–rebar strain curves obtained from the FE models is similar to the test results. However, overall the load–deflection curves obtained from the FE models are significantly stiffer than the experiments. This might be because the FE models were based on the smeared crack theory and used the perfect bond assumption. The concrete cracks could not have large crack openings in the simulations, while large crack openings and bond slip between concrete and steel cause large beam deflections and large rebar strains. However, the FE analysis provided good predictions of the ultimate load, close to the experimental results.

The patterns of cracks obtained from FE simulations were similar across the different cases, and the cases B16 and B16-6 at failure load are illustrated in Fig. 12. The planes of cracks within the concrete are represented by straight lines. These crack planes are perpendicular to the principal stresses that exceeded the concrete tensile strength. Under the applied type of loading, tension is induced in the rebar and the concrete elements in the upper part of the beam, especially around the connection due to high moment (longest moment arm length). When the tensile stresses in the concrete elements reach the tensile strength, flexural cracks are initiated and propagate to the lower part of the cantilever and to the main beam. The flexural cracks can be observed as a group of vertical lines. The tensile force in the steel rebar is also transferred to the surrounding concrete through the bonding and causes cracking of the surrounding concrete elements along the length of the rebar. The bond cracks can be observed as a group of short inclined lines along the length of the rebar.

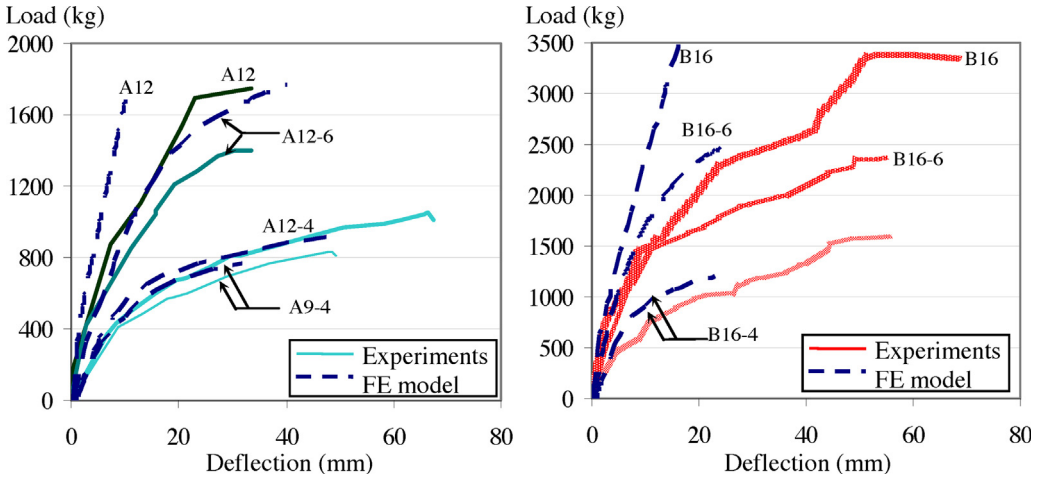

Fig. 9 – Comparison of the load–deflection curves between the experiments and the FE simulations: (a) A series, and (b) B series.

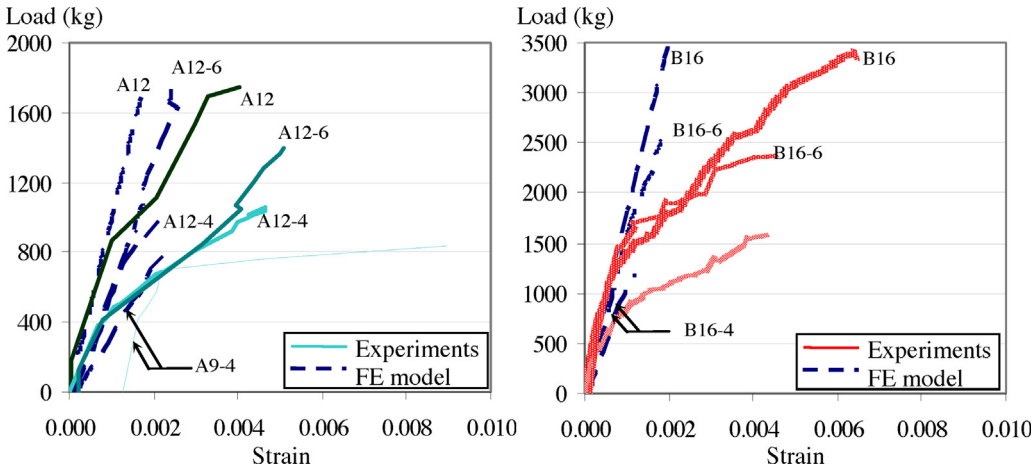

Fig. 10 – Comparison of the load–strain curves of the tension reinforcement between the experiments and the FE simulations: (a) A series, and (b) B series.

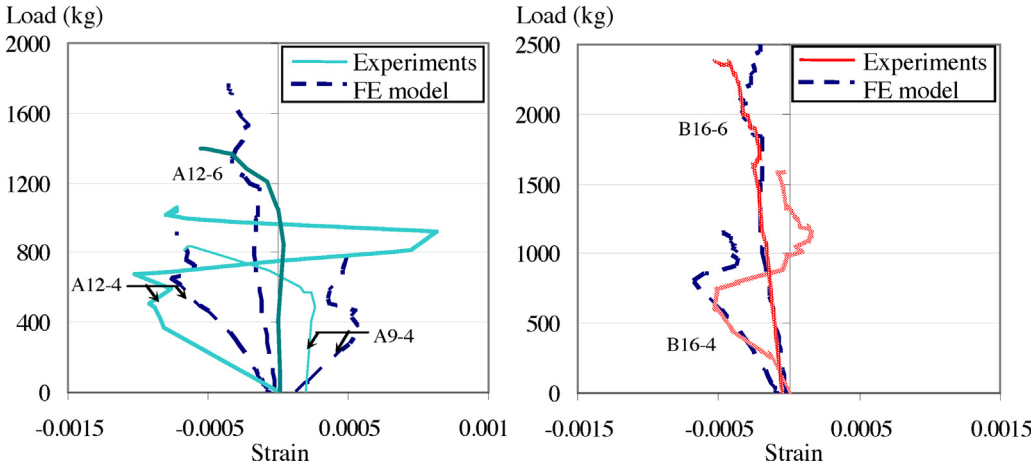

Fig. 11 – Comparison of the load–strain curves of the steel plate between the experiments and the FE simulations: (a) A series, and (b) B Series.

-Since the failure loads in the cast-in-place specimens are higher than those of the specimens with the welded plate joint, the tensile forces in the cast-in-place specimens are higher: flexural and bond cracks occurred more in the cast-in-place specimens. The cracks later propagated to the main beam around the connection and extended to the support. Normally, bond cracks are initially generated only at the interface between the rebar and the concrete cover [17,18], and sometimes are not observed in the actual beams. However, once the bond strength is reached, bond cracks may appear in the form of the tensile splitting cracks [19], as cracks in the upper part of the main beam. Concrete failure was clearly observed in simulated specimen B16, as shown in Fig. 12(a). On simulating specimen A12, concrete cracks occurred less due to smaller tensile forces. The simulated concrete failures agreed well with observations from the physical experiments.

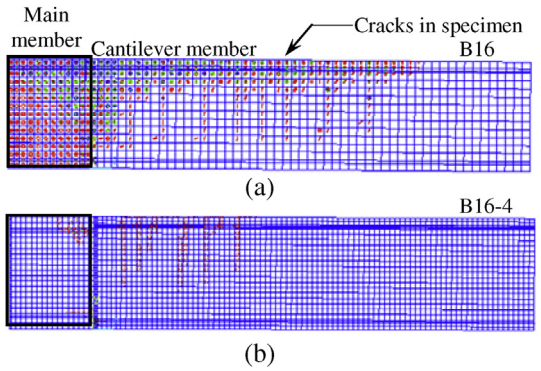

Fig. 12 – Crack patterns from the FE model at failure: (a) specimen B16, and (b) specimen B16-4.

Due to the lower loads at failure, the concrete cracks in the specimens with the welded plate joint were significantly less extensive than in the cast-in-place specimens, as shown in Fig. 12(b). Concrete cracks were clearly not the reason for failure in the specimens with the joint. Swelling of the plate and yielding of the rebars were found in the simulated case shown in Fig. 13. Transfer of tensile forces between the cantilever beam and the main beam caused swelling in the plate as shown in Fig. 13(a). The stress in the z direction (perpendicular to the plane of the plate, see Fig. 8) was

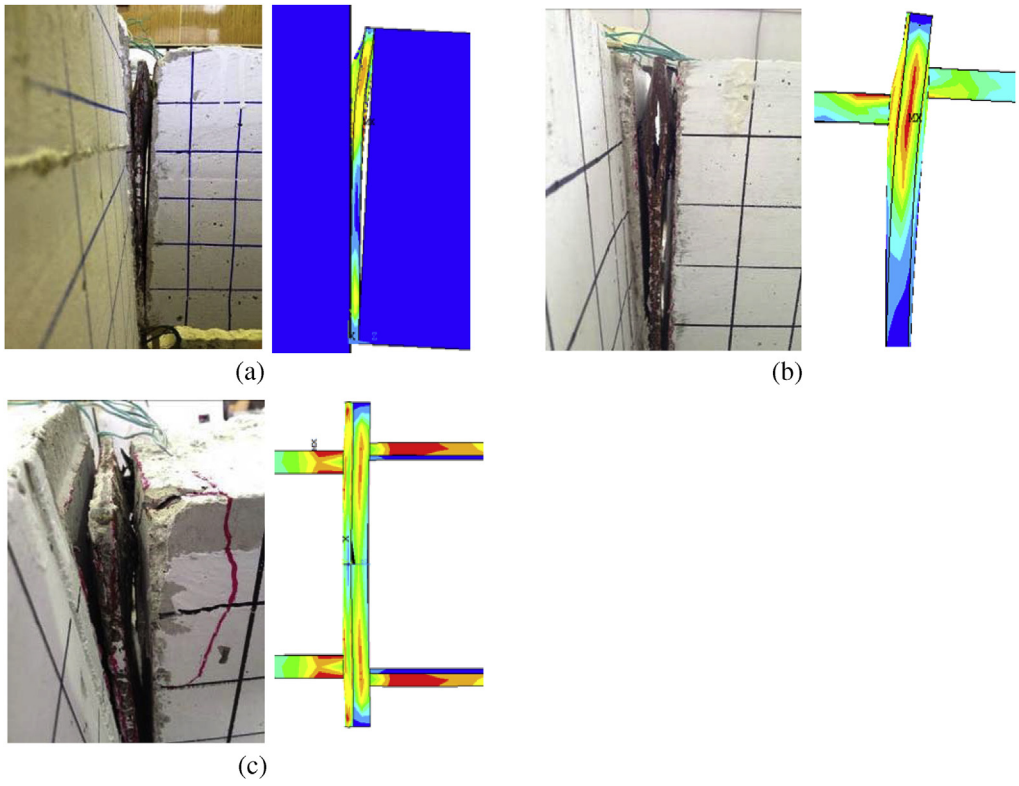

Fig. 13 – Failure modes at the welded plate joint compared between physical experiments and FE simulations with the stress in the z direction: (a) swelling of the plate (case A12-4), (b) yielding of the edge (case B16-6), and (c) yielding of the rebars (case A9-4).

maximum at the plate edge around the upper part, as shown in Fig. 13(b). The plate edges of specimens A12-4, A12-6, B16-4 and B16-6 reached their yield stress, which was the cause of failure. These welded plate failures could initiate splitting of the steel plates in the experiments. For specimen A9-4, the upper rebars reached their yield stress and caused the specimen failure, as shown in Fig. 13(c).

In summary, the computed load–deflection curves significantly differed from the experimental curves in terms of their slopes, probably due to the limitations of the analytical crack theory and to the bond assumptions in the simulation model. However, the FE model was still useful in predicting failure loads close to those observed experimentally. The overall failure modes in the FE simulations also agreed well with the experimental observations.

5. Design guideline proposal

To design a welded plate joint for required moment capacity, this study focuses on the rebar yielding (RY) and the welded plate failure (WPF). It is assumed that the welding between the rebar and the plate as well as between the plates is in good condition and can transfer the tensile and shear forces. Welding that satisfies such assumptions can be conducted through welding design and quality control, both in precast concrete factories and at construction sites. Furthermore, to simplify the design, the rebars in the concrete compression part are neglected on computing the moment capacity.

Consider a beam section subjected to a flexural load. The moment capacity of the section, M, depends on the force couple from compression resistance of the concrete section and tensile resistance of the rebars. However, as a practical way to avoid brittle failure, the compression resistance is designed to exceed the tensile resistance. The moment capacity is then controlled by the tensile resistance, F_t. To compute the moment capacity, the stress–strain distribution in a cross-section is graphically sketched in Fig. 14. The compressive stress distribution is assumed to be rectangular

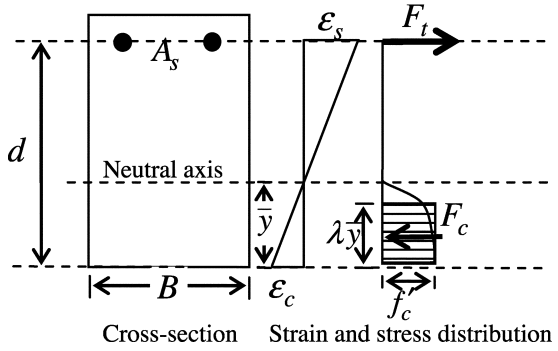

Fig. 14 – Stress–strain distribution in a reinforced concrete beam.

matching the compressive strength. $\bar{y}$ and $\lambda\bar{y}$ are the height and the effective height of the compression part, respectively. Due to the force equilibrium in the section, the compressive force F_c equals the tensile force F_t. The moment capacity can then be computed from Eqs. (1)–(3). For the load test in this study, the moment capacity, M, can be used to compute the load bearing capacity at the beam end, P, using Eq. (4).

$$M_c = F_t\left(d - \frac{\lambda\bar{y}}{2}\right) \tag{1}$$

$$F_t = F_c = B\lambda\bar{y}f_c' \tag{2}$$

$$\lambda\bar{y} = \frac{F_t}{Bf_c'} \tag{3}$$

$$P = \frac{M}{L} \tag{4}$$

where d is the distance from the rebar center to the edge of the compressive part, λ is the correction factor to provide the effective height of the compression part, set at value $\lambda = 0.8$ [20], B is the section width, f_c' is the compressive strength and L is the beam length.

Moment capacity of the welded plate joint is simply estimated based on Eq. (1). The tensile force, F_t, in Eq. (1) is substituted with the tensile resistance of the rebars, F_s, for rebar yielding, or with F_j for the case of welded plate failure. The tensile resistance of the rebars, F_s, is given in Eq. (5).

$$F_s = A_s f_y \tag{5}$$

where A_s is the rebar area and f_y is the yield stress of the rebars.

The tensile resistance of the welded plate, F_j, is considered through transfer of tensile forces between the rebars and the welded plate. To analyze this plate problem, fixed supports are assumed along the plate edge. The plate is pulled by the rebar forces and swells in two directions as shown in Fig. 15(a). In addition to shear forces and moment, the rebar forces also slightly contribute to in-plane forces and cause tensile forces at the supports. Based on plate geometry (height/width set to 2) and rebar locations of the specimens, the plate in its width direction (based on numerical estimates) resists 60–70% of the rebar forces. In other words, the tensile resistance of the welded plate, F_j, depends on the resistance in the width direction, and is about 60–70% of this. Since most of the forces are effectively resisted by the upper plate near the rebar location, the upper plate edges in the width direction are critical to failure.

To simply evaluate the tensile resistance of the plate, only the plate in the width direction is considered as a one-direction beam model with fixed ends as shown in Fig. 15(b). Depth and width of the beam model are the plate thickness, t_p, and the effective height of the plate, h_{eff}, respectively. Based on the numerical simulations done, the force resistance of the beam model is assumed to be 50% of the total plate resistance, and effects of the in-plane forces are neglected. Based on structural analysis, moment at the beam support is critical in Eq. (6) and reaches the plastic

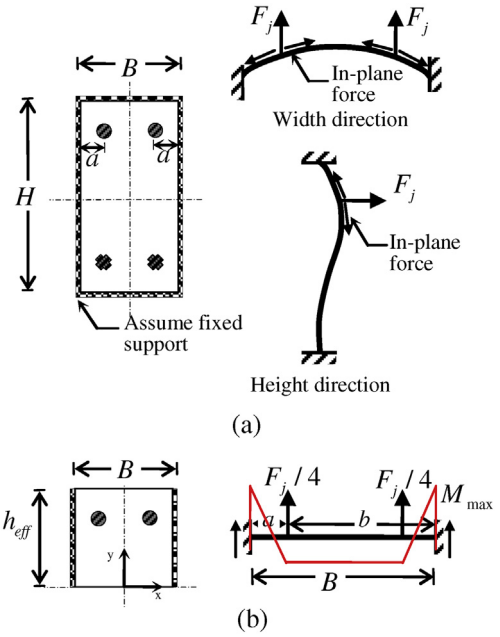

Fig. 15 – Plate problem: (a) plate deformation, and (b) simplified problem and its moment diagram.

moment resistance of the plate in Eq. (7). The location of the critical moment agrees well with the actual failures observed in the specimens. Eqs. (6) and (7) can be rearranged to compute F_j as in Eq. (8).

$$M_{max} = \frac{F_j/4}{B^2}(a^2b + ab^2) \tag{6}$$

$$M_p = \left(\frac{h_{eff}t_p^2}{4}\right)f_y \tag{7}$$

$$F_j = \frac{B^2 h_{eff} t_p^2 f_y}{(a^2b + ab^2)} \tag{8}$$

$$b = B - a \tag{9}$$

where a is the distance between the rebar center and the nearest plate edge in Fig. 15(a). Based on stress distributions in the FE models of the experiments, it was found that h_{eff} approximately varies with the plate height, H, and the rebar diameter, d_b, as in Eq. (10).

$$h_{eff} = H(0.15d_b + 0.35) \tag{10}$$

According to the finite element analysis, larger rebar diameters better transferred the rebar forces to the plate. Therefore, for the same plate height, larger rebar diameters provided deeper effective height of the plate.

The moment capacity due to the rebar yielding (RY) and the welded plate failure (WPF) can be computed by substituting F_t in Eq. (1) with the F_s in Eq. (5) or the F_j in Eq. (8). The moment capacities estimated with the proposed method, M_{PPM}, were validated against the FE simulation results, M_{FE}, and the physical test results, M_{test}. The labels used for each case were explained earlier in Section 2. There

Table 3 – Moment capacity and failure type.

Case	Moment capacity (kg m)				Failure type		
	Design based on the failure of		FE model	Test	Design	FE model	Test
	RY	WPF					
A9-4	1072	992	1327	1425	WPF	RY	RY
A9-6	1072	2181	1451	–	RY	RY	–
A12-4	2592	1037	1482	1818	WPF	WPF	WPF
A12-6	2592	2278	2505	2378	WPF	WPF	WR*
A16-4	4629	1094	1544	–	WPF	WPF	–
A16-6	4629	2398	2722	–	WPF	WPF	–
B9-4	1488	1717	1664	–	RY	RY	–
B9-6	1488	3803	1943	–	RY	RY	–
B12-4	3648	1792	1850	–	WPF	WPF	–
B12-6	3648	3968	3803	–	RY	WPF	–
B16-4	6656	1885	2083	2695	WPF	WPF	WPF
B16-6	6656	4168	4144	3935	WPF	WPF	WPF
C12-4	4691	2755	3284	–	WPF	WPF	–
C12-6	4691	6124	5282	–	RY	RY	–
C16-4	8635	2894	3355	–	WPF	WPF	–
C16-6	8635	6427	6504	–	WPF	WPF	–

Note: *WR is the welding failure at the rebar.

were 3 sections in the investigation, with the labels A, B and C corresponding to 150 × 300 mm, 200 × 400 mm and 250 × 500 mm cross sections, respectively. The comparison for validation is shown in Table 3, and graphically displayed in Fig. 16. In Table 3, the critical design moment capacity and the failure type are considered based on the lower value between the RY and WPF cases. The computed moment capacities conservatively agreed well with those from the FE models and the physical tests, in terms of both moment magnitudes and failure modes.

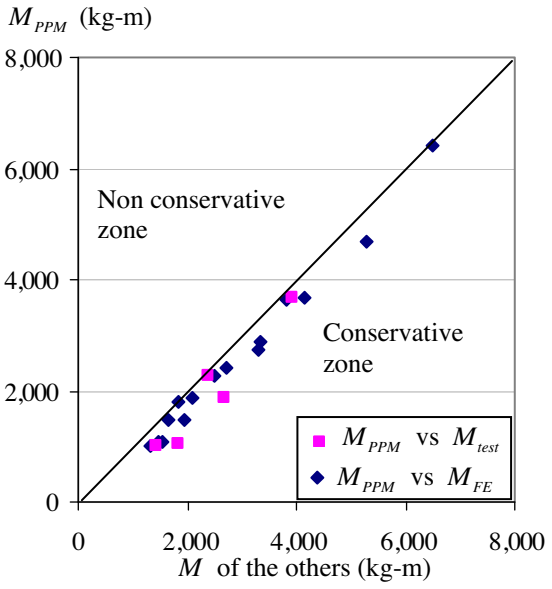

Fig. 16 – Comparison of proposed simplified estimates of moment capacity to finite element simulations and to physical test results.

6. Fire protection of the welded plate joint

To investigate failure behavior of the specimens with the welded plate joint under fire, a localized fire test at the joint was set up as shown in Fig. 17. To control the ambient fire temperature during the fire test, type K 4/0.32 GBS thermocouples with the sensitivity of 41 μV/°C (22.8 μV/°F) and the measurement range from −200 °C (−328 °F) to +1350 °C (2462 °F) were used. The thermocouples were installed at the joint surfaces as shown in Fig. 17. All tested specimens were prepared similar to B16-4, but with varying fire protections at the joint. The four alternatives for fire protection used in the investigation were: without any fire protection, with mortar plaster of 2.5 cm or 4 cm thickness, and with intumescent sealant of 1 cm thickness. Mortar plaster is considered a typical finishing for concrete members in structures. Intumescent sealant is a specific material used as a firestop material. The sealant is flexible and well suited for joints that must flex slightly. Specimens with plaster and with sealant are shown in Fig. 18(a). The cantilever beams were subjected to a 1 ton load at the end, giving a moment at about 60% of the moment capacity.

In the fire test, the specimens were exposed to fire from the bottom side for up to 120 min. Due to limitations of laboratory testing, this fire case was specified as a parametric fire matching the specifications in EN 1991-1-2 [21], as shown in Fig. 19. The parametric fire case uses the opening factor 0.037 $m^{1/2}$ and the thermal inertia 1960 J/m^2 $s^{1/2}$ K. Such factors are in a realistic range for a fire in an office or a house. This fire curve used is slightly less severe than the standard fire curves in EN 1991-1-2 [21] or ASTM E119 [22].

The fire resistance durations were 66, 113, >120 and >120 min for the specimens without fire protection, with thin plaster, with thick plaster, and with sealant, respectively.

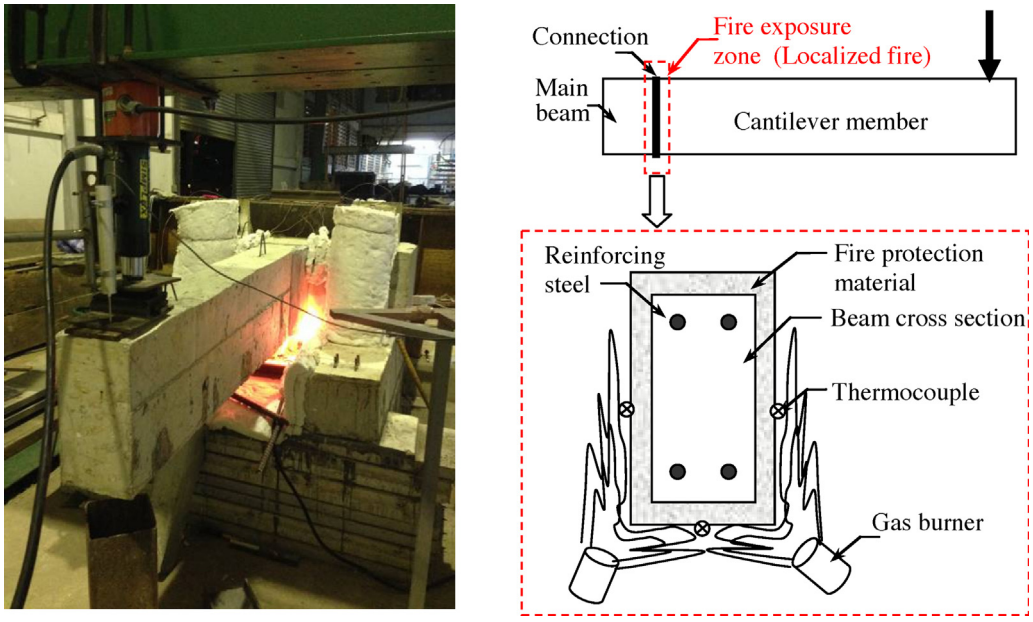

Fig. 17 – Fire test setup and location of temperature probe.

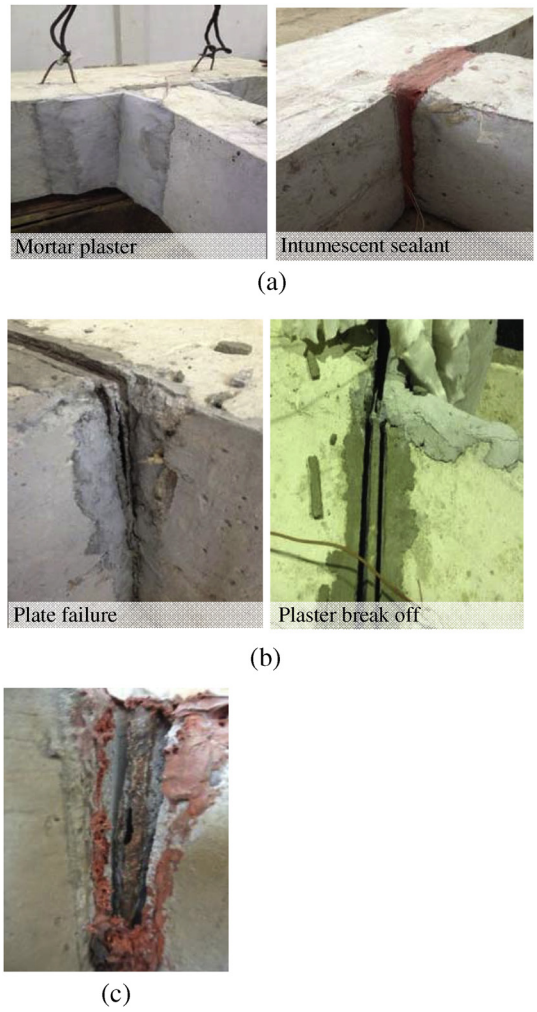

Fig. 18 – Fire test specimens: (a) fire protection, (b) failure of the specimen with thin plaster, and (c) damage in the specimen with sealant.

During the fire test, the deflection at the beam end gradually increased with fire duration, and increased significantly at failure. The failure modes were similar to the load tests without fire. A slight separation first formed between the cantilever beam, the joint and the main beam. After that, the plate swelled and later split at the upper plate edge, as shown in Fig. 18(b). Note that the mechanical degradation of the plate under high temperature degrades the moment capacity of the joint. Therefore, the joint can eventually fail even though the load was held constant during the fire test.

The separation causes breaking off of the plaster at the joint as shown in Fig. 18(b). The high temperature makes the plaster further crack due to thermal damage and expansion. Compared with thick plaster, a thin layer allows for more rapid thermal diffusion to the plate and faster degradation of the plate strength. Therefore, the joint separation and the plate swell were more severe with the thin plaster. Note that the degree of plaster breaking varied with the degree of separation. Since severe breaking off and cracking occurred in the thin

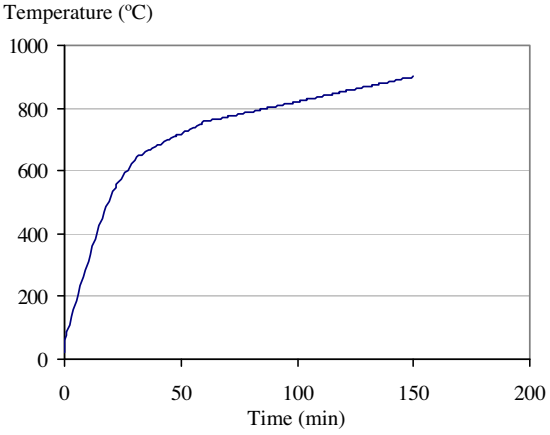

Fig. 19 – Parametric fire.

plaster, eventually the plate became directly exposed to fire, which contributed to specimen failure. Due to flexibility of the sealant, it was better able to cover the joint despite separation, and protected the joint against fire exposure. Breaking off of the sealant was not found during the fire test. After the fire test, the fire protections were removed from specimens that had not failed, in order to investigate residual damages. Only a small separation at the joint was observed in the specimen with thick plaster. A small split and swelling of the weld plated occurred in the specimen with sealant protection, as shown in Fig. 18(c).

In summary, thick plaster was the best alternative for preventing joint damage. However, thick plaster may not be practical and is costly. Therefore, flexible sealant as the fire protection material is recommended for the welded plate joint.

7. Discussion and conclusions

Structural behavior of a loaded cantilever with welded plate joint and its fire resistance while subjected to a flexural load were examined. The investigated specimens were reinforced concrete (RC) cantilever beams connected to an RC main beam with welded plate joints. Seven load tests and four fire tests were conducted as physical experiments. The varied parameters of the load tests were joint section dimensions, plate thicknesses, and rebar dimensions, in such ranges that are practical for use in small construction. Furthermore, finite element simulations of the specimens were used to assess in detail the structural behavior, and partly based on these simulations a simplified method was devised to estimate the moment capacity of a welded plate joint. However, further experiments on thicker plate are required to investigate an improvement of the moment capacity. The main conclusions are as follows:

- The load bearing capacity of a joint depends on its ability to resist the tensile forces induced in the steel rebars. Separation and swell of the joint occur when the load becomes excessive. The main failure of the welded plate joint was splitting of the plate. However, once the welded plate can resist higher tensile forces than the connected rebars, the joint will failed from tensile yielding in the rebars.
- The ultimate loads for the specimens with welded plate joints using 4-mm and 6-mm thick plates were about 50% and 70% of those for cast-in-place specimens, respectively. Slopes of the load–deflection curves, which represent stiffness of the joint, mainly increased with plate thickness, not with the diameter of the reinforcement. The initial stiffness is closely similar to the cast-in-place specimens for the thicker plate, whereas it is degraded for the thinner plate.
- The numerically simulated load–deflection curves significantly differed from the experimental deflections, due to limitations of analytical crack theory and bond assumptions made in the simulation model. However, overall the failures of the finite element (FE) models agreed well with the experimental observations.
- To simply evaluate tensile resistance of the welded plate, only the plate in width direction was considered as a beam model with fixed ends. Based on numerical simulations, the force resistance of this beam model was assumed to be 50% of the total welded plate resistance. Based on structural analysis, the moment at the beam ends was critical, and this was used to compute the moment capacity. The moment capacity estimates with the proposed method agreed well with those from the FE model and with the experimental observations, in terms of moment magnitudes and failure types.
- Alternative fire protections investigated were: without any fire protection; with thin or thick mortar plaster; and with flexible sealant. The thick plaster and the sealant did the best in preventing joint damage and had fire resistances in excess of 2 h. Due to the joint separation, breaking off and cracking of the thin plaster contributed to specimen failure, while the thick plaster coped better in these respects. The flexible sealant protected the joint from fire exposure by extending itself to cover the joint even with some joint separation.

To promote safe joints in precast concrete construction, understanding the joint behavior and design methods for moment capacity requirements are necessary. The proposed method allows simple and practical estimates of the moment capacity. As usual, the design equations rely on nominal capacities, and safety factors reducing the nominal strength must be applied in practical design, to provide a margin of safety. For fire safety, the welded plate joints are the weakest link in the system. Without their fire protection, steel members may quickly fail under severe fire. Since joint separation may occur during flexural load bearing, rigid fragile protection such as plaster is not practical for a welded plate joint, instead flexible fire protection material is recommended for use with this type of joints.

Acknowledgments

This work was financially supported by the Thailand Research Fund (TRF) and by the Prince of Songkla University: Research Grant for New Scholar (TRG5780109). We would like to sincerely thank the copy-editing service of Research and Development Office, and Assoc. Prof. Dr. Seppo Karrila who dedicated his time to provide valuable comments, and gratefully acknowledge the support and assistance received.

REFERENCES

[1] H.H. Korkmaz, T. Tankut, Performance of a precast concrete beam-to-beam connection subject to reversed cyclic loading, Engineering Structures 27 (2005) 1392–1407.
[2] M. Seckin, H.C. Fu, Beam–column connections in precast reinforced concrete construction, ACI Structural Journal 87 (3) (1990) 252–261.
[3] K. Soubra, J.K. Wight, E. Naaman, Fiber reinforced concrete joints for precast construction in seismic areas, ACI Structural Journal 88 (1) (1991) 214–221.

[4] A.A. Mandt, Moment rotation effects on the stability of columns in precast concrete structures, Ph.D. thesis, University of Nottingham, United Kingdom, 1992.
[5] H. Gorgun, Semi-rigid behavior of connections in precast concrete structures, Ph.D. thesis, University of Nottingham, United Kingdom, 1997.
[6] R. Ragupathy, Semi-rigid connections in precast concrete frames, Ph.D. thesis, City University, Northampton Square, United Kingdom, 1993.
[7] K.S. Ellioll, G. Davies, H. Gorgun, M.R. Adlparvar, The stability of precast concrete skeletal structures, PCI Journal 43 (2) (1998) 42–60.
[8] M.E. Rodríguez, M. Torres-Matos, Seismic behavior of a type of welded precast concrete beam-column connection, PCI Journal 58 (2013) 81–94.
[9] M. Zermeo, A. Fuentes, C. Aire, Cyclic lateral load response of beam–column connections for precast construction, Internal Report 1704, Instituto de Ingeniea, UNAM, Mexico City, Mexico, 1992.
[10] S.A. Bilgin, Behavior of dry joints under seismic action, M.Sc. thesis, Ankara: Department of Civil Engineering, Middle East Technical University, Turkey, 1986.
[11] T. Tankut, U. Ersoy, Precast concrete members with welded plate connections under reversed cyclic loading, PCI Journal 38 (4) (1993) 94–100.
[12] N. Boonklom, Companion of beam-column connection strength using steel plate and cast-in-place connections, Master thesis, Construction Engineering Technology King Mongkut's University of Technology North Bangkok, Thailand, 2010.
[13] J. Thawonpaisanchewa, Structural behavior and proposed design equations for prefabricated beam-column connections, Master thesis, Civil Engineering King Mongkut's Institute of Technology North Bangkok, Thailand, 2006.
[14] ANSYS, ANSYS Multiphysics, Version 11.0 SP1, ANSYS Inc., Canonsburg, PA, 2007.
[15] CEN (European Committee for Standardisation), EN 1992-1-2, Eurocode 2: design of concrete structures, Part 1.2: general rules-structural fire design, British Standards Institution, London, 2004.
[16] S. Zhou, D.C. Rizos, M.F. Petrou, Effects of superstructure flexibility on strength of reinforced concrete bridge decks, Computers & Structures 82 (1) (2004) 13–23.
[17] T. Pothisiri, P. Panedpojaman, Modeling of mechanical bond–slip for steel-reinforced concrete under thermal loads, Engineering Structures 48 (2013) 497–507.
[18] P. Dybeła, K. Furtakb, The effect of ribbed reinforcing bars location on their bond with high-performance concrete, Archives of Civil and Mechanical Engineering 15 (4) (2015) 1070–1077.
[19] P. Panedpojaman, T. Pothisiri, Bond characteristics of reinforced normal-strength concrete beams at elevated temperatures, ACI Structural Journal 111 (6) (2014) 1351–1362.
[20] CEN (European Committee for Standardisation), EN 1992-1-1, Eurocode 2: design of concrete structures, Part 1.2: general rules and rules for buildings, British Standards Institution, London, 2004.
[21] CEN (European Committee for Standardisation), EN 1991-1-2, Eurocode 1: actions on structures – Part 1.2: general actions – actions on structures exposed to fire, British Standards Institution, London, 2004.
[22] ASTM, Standard test methods for fire tests of building construction and materials, ASTM E119, West Conshohocken, PA, 2007.